ELSEVIER
Physica D 2857 (2002) 1–16
PHYSICA D
www.elsevier.com/locate/physd

Shock bowing and vorticity dynamics during propagation into different transverse density profiles

K. Kremeyer [a,*], S. Nazarenko [b], A.C. Newell [a,b]

[a] *Department of Physics, University of Arizona, PAS 358, Tucson, AZ 85721, USA*
[b] *Mathematics Institute, University of Warwick, Coventry CV4 7AL, UK*

Received 15 October 2000; received in revised form 29 November 2001; accepted 30 November 2001

Communicated by I. Gabitov

Abstract

A 2D numerical investigation is presented of shock wave propagation into a gas whose density is modulated in the transverse direction across the width of a shock tube. These density modulations represent temperature distributions in which low density corresponds to high temperature gas and high density corresponds to low temperature gas. This work is motivated by recent shock-plasma experiments, and mechanisms to explain the experimentally observed shock "splitting" signatures are investigated. It is found that the shock splitting signatures are more pronounced when the shock wave is more strongly curved or bowed. This occurs as the depth of the initial density profile is increased. The gross features of the shock splitting signatures are relatively insensitive to variations in the shape of the initial density profile (into which the shock propagates). Several interesting features of vorticity production and evolution are also indicated. © 2002 Published by Elsevier Science B.V.

PACS: 47.40.-x (Compressible flows, shock and detonation phenomena); 52.35.T (Shock waves in plasma); 47.20.-k (Hydrodynamic stability); 47.32.-y (Rotational flow and vorticity)

Keywords: Curved shock; Vorticity; Jet; Richtmyer–Meshkov instability

1. Introduction

Experimental and theoretical work on using plasmas to reduce drag on airplanes has experienced a resurgence after Klimov et al. [1,2] reported on their plasma wind tunnel experiments performed in Russia. According to Klimov et al., a significant drag reduction was observed on a cone-shaped model in supersonic flow when plasma was added ahead of the shock. In supersonic flows the major contribution to the drag comes from the bow shock (wave drag). Thus, the attention of Klimov et al. was given to measuring the shock wave modifications after the plasma injection. The shock was observed to decay and the usually sharp jump in density at the shock front "split" into two or more smaller jumps. Significant experimental progress has been made over the past 2 years in the USA, UK and Russia [3]. However, an outstanding issue still is whether the observed shock "splitting" and attenuation are due to plasma electromagnetic effects, or to the gas heating which accompanies the introduction of nonequilibrium plasmas, or a combination of both. It is the purpose of this paper to show that much

* Corresponding author.
E-mail address: kevin@physics.arizona.edu (K. Kremeyer).

PII: S0167-2789(02)00348-2

of the observed behavior in the experimental data can be explained by gas dynamics as long as one takes account of the fact that the dynamics is not simply one-dimensional (1D).

To understand better the main physical processes leading to bow shock modification and dissipation, the experimental and theoretical foci have been on simple plasma-shock systems rather than on realistic vehicle shapes where the essential physics can be obscured by more complicated flows. Shock tube experiments, in which a shock propagates though a discharge plasma, are an example of such a basic system. The shock tube geometry is simpler than the supersonic flows around cones and wedges, and the relevant gas dynamics and plasma physics is easier to study. Motivated by Klimov et al., Ganguly et al. [4] observed shock splitting and damping in a shock tube containing an argon plasma. Although the shock tube geometry is relatively simple, there are a number of difficult diagnostic issues in these experiments, including the determination of the temperature distribution of the gas within the tube. As our numerical study shows, the shock behaves differently as it propagates into different temperature distributions, and an accurate knowledge of certain aspects of the true distribution is vital to any effort to model these dynamics carefully. One of the main experimental diagnostic tools used to characterize the flow within the tube made use of a laser beam to measure density gradients along the tube axis. The laser beam was pointed across the tube, transverse to the tube axis. The laser beam will bend towards the highest density neighboring path because this path will also have the highest refraction index. The beam deflection therefore serves as an approximate measurement of the first derivative (taken along the tube axis) of the gas density integrated across the tube cross-section. The laser diagnostic technique took advantage of this effect and the deflection of the laser beam was measured as the shock passed across it [4]. A notable result of increasing the current density in the shock tube experiment was that the characteristically sharp density increase across a shock (with the corresponding single sharp spike in laser beam deflection) became more gradual. This was indicated by a “broad” spike in laser deflection which was generally modulated by two or more “sub-jumps” within the broadened structure. The puzzle at hand has been to explain the nature of this shock broadening or splitting.

Very soon after the first experiments, it was realized that the electron gas energy is many orders of magnitude less than the energy of the neutral component and therefore cannot be important in the shock dynamics. On the other hand, it was demonstrated that the experimentally observed results could not be explained with a 1D model, given only the heating associated with the discharge [4]. This led many researchers to search for a “plasma magic”, and this search continues up to the present day. Hilbun et al. showed, however, that the disagreement with the gas dynamics is removed when the multi-dimensionality of the problem is taken into account [3] (section GG, Vol. 2). To model the transverse temperature distribution, Hilbun et al. numerically modeled the two-dimensional (2D) gas flow in this geometry. They showed that much of the experimental shock behavior can be replicated without including ionization by assuming an equilibrated temperature distribution (given by iterating Laplace’s equation with fixed boundary conditions and source terms). With this temperature distribution, strong shock broadening/splitting was not apparent, although weak transverse flow within the shock tube demonstrated the two-dimensionality of the dynamics.

Hilbun et al.’s numerical experiments clearly indicate that two-dimensionality of the flow is important, and that this two-dimensionality is key in the lack of agreement between the experimentally measured shock speed and the predictions of 1D models. However, the calculation of the initial temperature distribution greatly simplifies the heating mechanism and does not account for the cooling gas flow that was present in the tube. In addition, the reported numerical results did not demonstrate the observed shock splitting.

The work reported in this paper is not intended to model the experiments exactly (e.g. by improving the temperature distribution model associated with the argon discharge). Instead, the goal is to examine the cases corresponding to a large set of initial temperature profiles which differ from each other in amplitude, characteristic width and shape. The results demonstrate the robustness of the shock splitting and other observed phenomena, by virtue of their low sensitivity to the detailed shape of the initial density profile [5]. We also discuss the baroclinic vorticity generation; the instability of lagging interfaces evolving into mushroom-like structures (similar to the Richtmyer–Meshkov instability), and the formation of quasi-1D jet-like velocity and density profiles immediately behind the shock [6]. It will be shown that vorticity plays the key role in the observed shock modifications. Because the minimal number of dimensions where these effects can be captured is 2, we examine the 2D case. Our aim is not to reproduce the experimental results exactly, but rather to understand and to explain qualitatively the general features observed. The results presented here indicate that the experimentally observed shock splitting signatures can be fully attributed to the shock curving or bowing as it passes through the different transverse density (temperature) profiles. This assertion is further validated by recent experimental/computational comparisons [7].

2. Physical model

The goal of this study is to concentrate on the shock modifications due to the combined effects of the temperature gradients and 2D flow using the simplest possible model. To achieve this, the 2D compressible Euler equations were evolved on a rectangular domain representing the shock tube. These equations neglect both viscosity and heat conduction, resulting in simpler computational and analytical modeling.

The Euler equations used in this study are

$$-\frac{\partial \rho}{\partial t} = \frac{\partial(\rho u)}{\partial x} + \frac{\partial(\rho v)}{\partial y}, \tag{1}$$

$$-\frac{\partial(\rho u)}{\partial t} = \frac{\partial(P + \rho u^2)}{\partial x} + \frac{\partial(\rho u v)}{\partial y}, \tag{2}$$

$$-\frac{\partial(\rho v)}{\partial t} = \frac{\partial(\rho u v)}{\partial x} + \frac{\partial(P + \rho v^2)}{\partial y}, \tag{3}$$

$$-\frac{\partial E}{\partial t} = \frac{\partial(u(E + P))}{\partial x} + \frac{\partial(v(E + P))}{\partial y}, \tag{4}$$

where P is the pressure, ρ the density, u the x-component of the fluid velocity, v the y-component of the fluid velocity and E the energy per unit volume. An equation of state completes the description, which for this study, is the ideal gas law (with $\gamma = 1.4$ for a diatomic gas)

$$P = (\gamma - 1)[E - \tfrac{1}{2}\rho(u^2 + v^2)]. \tag{5}$$

2.1. 1D dynamics

First, it will be helpful to briefly summarize the behavior of 1D shocks. The simplest initial condition is for two constant states of infinite extent in either direction to be separated by a finite pressure discontinuity: a classical Riemann problem. The solution (Fig. 1) is a shock wave propagating into the low pressure state at constant velocity, and a rarefaction wave broadening and propagating/eroding into the high pressure state. Between these two waves, which are moving apart, the solution calls for two new constant states differing only in their densities [8,9]. The discontinuity separating these two intermediate states is called a contact surface; it is characterized by no pressure discontinuity; and moves with the fluid speed (which is also continuous across it). Often, the main states of interest are the states immediately ahead of and behind the shock wave. The Rankine–Hugoniot conditions relate the fluid parameters in front of the shock to those behind the shock in terms of the Mach number. To mimic this simple theoretical situation, experiments are often performed in a shock tube by separating the tube (with a thin membrane) into two parts with different pressures. Breaking the membrane then allows the gas from the higher pressure section to flow into the lower pressure section, and the formation and propagation of a shock wave can be observed. Disregarding the initial region of the breaking membrane and the effects of the tube walls, the experiment is very nearly 1D and the results agree well with the 1D theory.

The 1D case described above is simple because all the parameters are clearly defined. Ahead of the shock, there is a single clearly defined pressure (P), density (ρ), ratio of compressibilities (γ), and speed of sound (c). As a result, the Mach number (M) of the constant

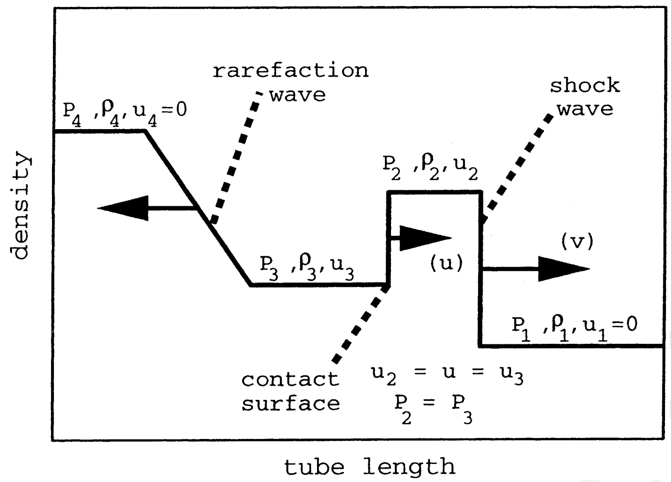

Fig. 1. The 1D Riemann problem.

velocity (v) shock is also well defined as v/c. For the system presented in this paper, when a shock propagates into an inhomogeneous medium with a nonconstant density/temperature distribution, there is ambiguity as to which parameters to assign to the states used in a 1D analysis. For a shock moving with a constant velocity through a nonconstant transverse density profile, an obvious ambiguity occurs in how to assign an appropriate Mach number. The shock speed (v) is constant, while the sound speed (c) ahead of the shock varies with the density. To simplify the analysis of such experimental shock measurements, average parameters are often taken to characterize the states ahead of a shock, and the 1D theory and "averaged" Rankine–Hugoniot conditions are applied. The work presented here demonstrates that this practice can lead to erroneous results.

2.2. 2D effects

The main problem with simply averaging over the fluid parameters of the system and then applying the 1D fluid equations is that the effect of transverse gradients in the fluid velocity are ignored. Such effects arise when a shock passes over an inhomogeneity. For example, if a shock passes over a pocket of hot (low density) gas, the gas in this low density pocket will be pushed forward at a velocity greater than that of the heavier neighboring gas. Conversely, gas in a cold (high density) pocket will move forward less quickly than the warmer neighboring gas. A shock encountering such inhomogeneities, therefore, results in localized gradients in the fluid velocity, where pockets of gas are preferentially flowing faster (for light/hot pockets) or slower (for heavy/cold pockets) than the average gas velocity behind the shock. These are localized examples of jet-like flow. It is precisely the effect of such jet-like flow which is not accounted for when using the averaged 1D fluid equations. Such situations arise in many laboratory experiments and, in particular, when shocks propagate through a weakly ionized plasma in shock tubes. In these experiments, ionization is accompanied by a commensurate heating of the gas [1,2,4]. Since the shock tube walls remain cooler than the heated gas, gradients arise in the temperature (and therefore, density) along the tube cross-section. The shock is then observed as it propagates down the tube (perpendicular to these density gradients). These experiments have provided an excellent set of illustrative examples for which the 1D equations are unable to predict shock speeds or explain the observed propagation, while 2D simulations match the observations well [6,10].

In studying the propagation through the nonuniform temperature profiles, our attention has been concentrated on the generation of vorticity ($\vec{\omega} = \vec{\nabla} \times \vec{v}$) and the subsequent 2D vortex dynamics which is crucial for understanding the observed flow. Vorticity is generated at the shock via the mechanism described by the baroclinic source term which has the following form [11]:

$$\left(\frac{\partial \vec{\omega}}{\partial t}\right)_{\mathrm{B}} = \frac{\vec{\nabla}\rho \times \vec{\nabla} P}{\rho^2}. \tag{6}$$

The baroclinic vorticity generation term describes the jet-like flow which occurs when a shock passes across density variations. This term is expected to be rather small in regions with smoothly varying flow parameters, and large only at discontinuities [6]. In particular, it will be important at the shock front (via the pressure discontinuity) and the trailing surface (mostly via a density jump).

3. Numerical model

This paper investigates a shock propagating into a gas of nonuniform density in an elongated 2D rectangle which is the simplest model for a cylindrical shock tube. As we mentioned in Section 1, 2 is the minimal number of dimensions which can capture the important effects of vorticity generation and jet formation. We consider the 2D model because it is easier to compute numerically and because the vortex dynamics is easier to visualize and describe theoretically. The simulation is performed using a 2D conservative Euler code to solve Eqs. (1)–(5). This algorithm is described in [12]. The time-step method is third-order Runge–Kutta, and a fifth-order weighted essentially nonoscillatory (wENO) scheme is used to obtain the fluxes between grid points. The consistence and convergence of this scheme have been thoroughly investigated by Jiang et al. [12,13].

There are three ghost points outside each of the boundaries of the computational domain. The boundary conditions at the top and bottom boundaries are “reflecting, slip”, and represent the walls of the shock tube. The left and right boundaries are maintained at two distinct time-independent states. These time-independent states initially extend into the shock tube and are joined by a discontinuity near the left end of the computational domain. The initial state on the left side of the tube is the high-pressure state and is the same for all of the results reported in this paper. It has a constant pressure of 1.0 and a constant density of 1.0 (in dimensionless units), and the *x*- and *y*-components of the velocity are both 0. When the flow begins, the rarefaction wave propagates away from the domain to the left, and the shock wave propagates to the right, followed by the density discontinuity (see Fig. 1 for the 1D analogs).

The right-hand side initial state always has a pressure of 0.1, 0 velocity, and one of the transverse density profiles discussed below. The selected gas states, into which the shock propagates, are not meant to be an exact model of any specific experiment, but to demonstrate the effect of different transverse density gradients and distributions on the shock dynamics.

This was done by propagating shocks through a variety of simple density profiles shown in Fig. 2A–C, which are supposed to span the spectrum of possible transverse density distributions. For the top-hat distributions (Fig. 2A and B), the maximum gradient occurs when the distinct densities at the tube wall and tube axis meet discontinuously. The top-hat distribution was not truly discontinuous, but was smoothed by using the tanh function. This ensured that the chosen configuration was preserved and resolved upon changing grid resolution. A sharp density change of the top-hat profiles is relevant given the presence of a substantial cold boundary layer at the walls of the shock tube. Such a boundary layer is more prevalent in the experimental geometry of Ganguly et al. [4] as the flow rate of cooling gas is increased.

A V-shaped density distribution (in Fig. 2C) was also used, since it allows a simple analytical calculation of the baroclinic vorticity generation at the shock due to the (piece-wise) constant density gradient associated with the V-shape. In addition, the V-shaped distribution represents the shallowest density gradient necessary to connect the high density at the tube walls

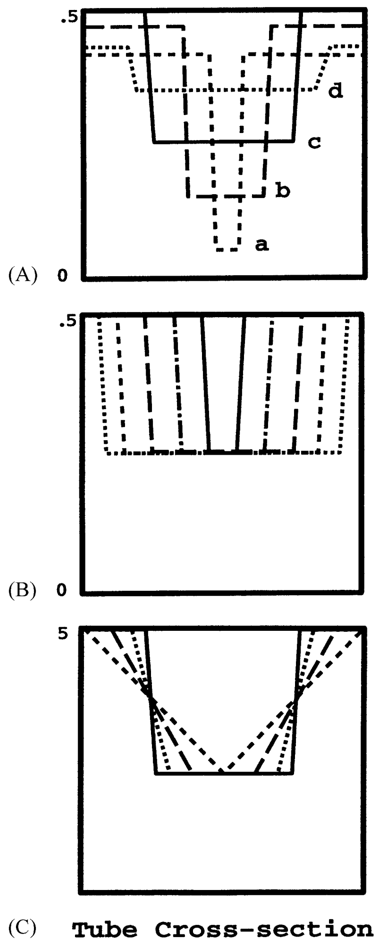

Fig. 2. Three different sets of initial density profiles used in simulations: (A) top-hat profiles with fixed area; (B) top-hat profiles of fixed depth; (C) constant area profiles with shapes ranging from top-hat to the V-shape.

with the low density on the tube axis. We also used a range of transitional shapes, between the top-hat and the V-shapes, which are shown in Fig. 2C.

Finally, we used Gaussian density distributions as a reasonable and smooth representation of a low temperature at the tube walls with a higher temperature on the tube axis. Together with the shapes shown in Fig. 2A–C, such a choice of the initial density profiles is aimed at spanning all possible situations that may appear in experimental conditions in order to establish the physical effects that are common and relatively insensitive to the initial shape.

Although the convergence of the numerical scheme has been thoroughly demonstrated by Jiang et al. [12,13], it was further substantiated in this study on the deepest top-hat distribution described in Fig. 2A to allay any concerns over the sharp gradients. Fig. 3 shows a specific density cross-section simulated on the 2D domain using different grid spacings (80, 160, 320 and 640 grid points across the tube). The cross-section exhibiting the most detailed and discontinuous distribution was selected. One can see in Fig. 3 that even for this extreme density gradients the numerical method is convergent.

4. Results

4.1. Shock profiles

The goal of this investigation is to show, by using a variety of initial density profiles, the robust quality of the features observed in the ensuing dynamics. Vorticity generation at the shock and how it redistributes behind the shock is the key element and, in addition to the explanation of shock splitting, is the main new understanding arising from the present work.

There were two basic profiles considered, the V-shape and the top-hat. As mentioned already, the V-shape represents the shallowest density gradient needed to connect the high density wall region to the interior. Moreover, it is amenable to analytical calculations. The top-hat profile was used to address the suggestion that a cold gas layer at the wall may result in a bowing of the shock strong enough to explain the experimentally observed splitting [14]. To simulate the most extreme example of this, a high density (low temperature) gas at the tube walls was joined discontinuously with a low density (high temperature) gas at the tube center. This was done purposely to exaggerate the effects of density differences/gradients. Some different top-hat density profiles are shown in Fig. 2A. The series of simulations of shocks propagating through these four profiles will be used to illustrate how the different 2D shock shapes and density distributions translate into “split” signatures in the laser diagnostic technique used by Ganguly et al.

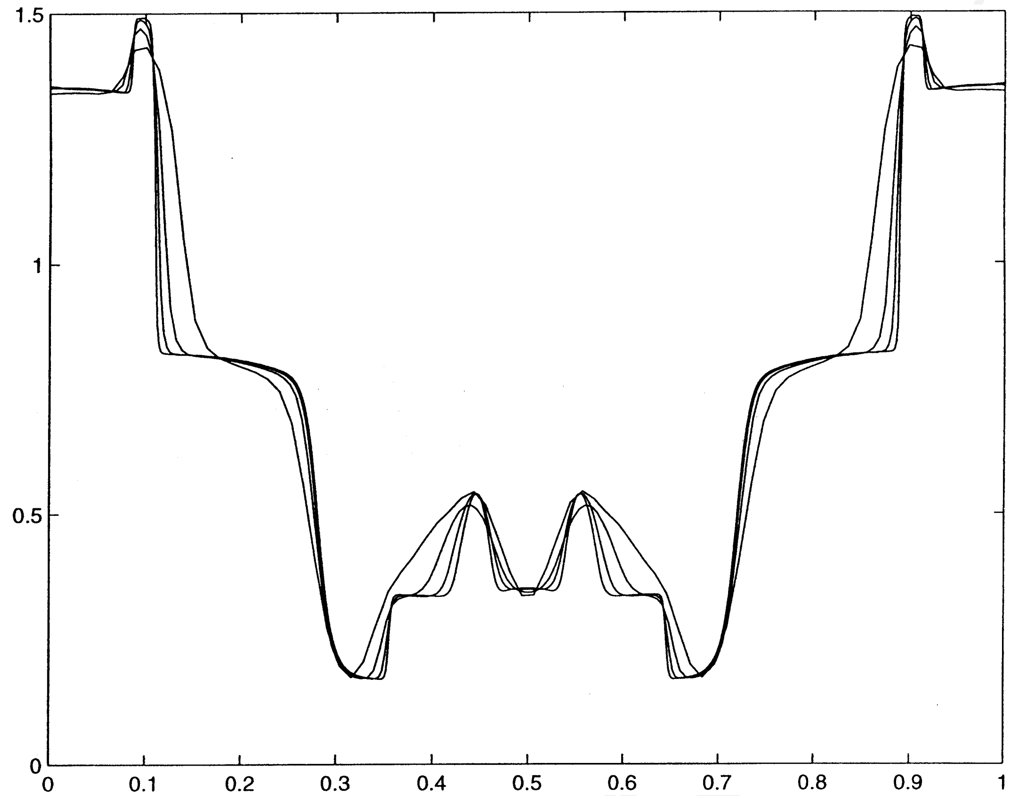

Fig. 3. A density cross-section from behind a shock (propagating into the deepest top-hat profile shown in Fig. 2A) is taken from 2D simulations at four resolutions: 80, 160, 320 and 640 grid points across the tube, respectively.

Physically, the top-hat profiles correspond to hot gas in the center of the tube, discontinuously meeting cold gas at the walls of the tube. The different high and low density values have been selected to maintain the average density across the tube equal to 0.375. This is the same as the average density for a V-shaped profile connecting a density of 0.5 at the walls to a central density of 0.25 (which was investigated in [6]).

Fig. 4 shows the 2D contour plots of density after a shock has propagated into the different initial density distributions of Fig. 2A for times after which the main qualitative features have developed. Immediately behind the shock, the density is lowest on the center line and it grows toward the walls. As in 1D, the density increase caused by the shock is followed by a density decrease behind the lagging surface (compare with Fig. 1). One can see that the shock wave becomes more curved or “bowed” when propagating into the deeper/narrower profiles. One can also see in Fig. 4a–c that a region in the middle of the tube can be shockless if the incoming gas at this location is hot enough (e.g. for deep profiles). However, the shock is always present at the sides where it contacts the wall either at a right angle (sometimes branching into a Mach stem) or with a reflected shock (for large enough bowing angles).

The shock bowing (shown, e.g. in Fig. 4d) occurs because of the jet that forms behind the shock as explained in the beginning of Section 2.2. We found that such a jet is very stable and it often extends for long distances behind the shock without significant variations in longitudinal direction. A manifestation of such quasi-1D structures can be seen, e.g. on the density profiles in Fig. 4c and d.

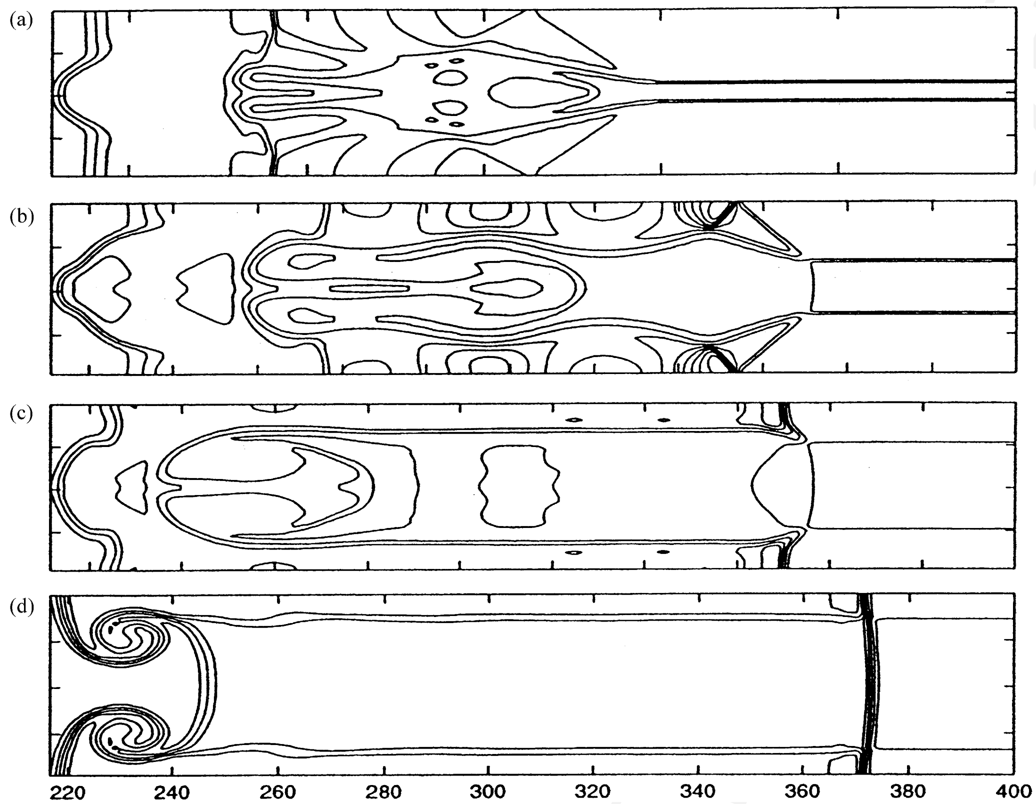

Fig. 4. Density contour plots from four simulations corresponding to four top-hat profiles shown in Fig. 2A. Immediately behind the shock, the density is lowest on the center line and it grows toward the walls. As in 1D, the density increase caused by the shock is followed by a density decrease behind the lagging surface (compare with Fig. 1).

A particular example of the vorticity, velocity, density and pressure profiles associated with the 1D jet structure is shown in Fig. 5. Here the results shown correspond to the run with the V-shape initial profile (shown in Fig. 2C). We have chosen the V-shape because it allows an analytical calculation of the vorticity generated at the shock. However, jets that appear for the top-hat shapes are qualitatively similar to the one corresponding to the V-shape. The 1D jets and their relation to the vorticity generation will also be discussed in Section 4.2.

Fig. 6 shows four plots, corresponding to the four different simulations in Fig. 4. However, in this case they have been run to precisely the same moment in time. The top curve of each plot represents the density, integrated/averaged across the tube cross-section, and is roughly proportional to the effective index of refraction seen by a diagnostic laser. The bottom curve is the first derivative (along the length of the tube) of the averaged density (shown in the top curve), and is roughly proportional to the laser deflection measurement reported by Ganguly et al. [4]. The shock splitting effect is most clearly seen in Fig. 6c. The initial jump in density occurs when the laser beam first encounters the shock. At this point, the shock is perpendicular to the tube axis (tangent to the laser beam), and the resulting rise in density next to the beam is very sudden. This results in a strong deflection of the beam into the higher density gas. As the curved portion of the shock continues to cross the laser's path, the rise in average density is more gradual (due to the oblique nature of the shock) and a smaller laser deflection is registered. The largest and most sudden jump occurs when the portion of the shock wave next to the walls

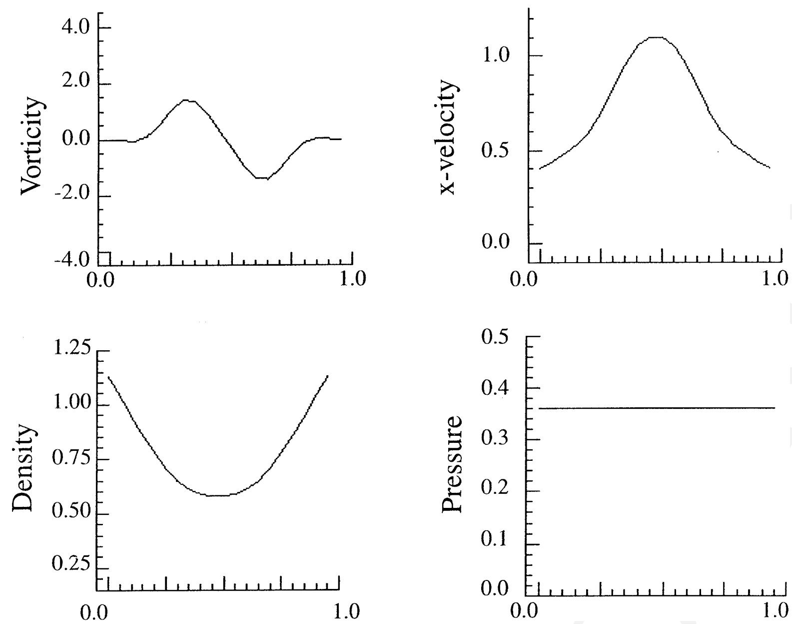

Fig. 5. Cross-sections of vorticity, density, the *x*-velocity and pressure corresponding the quasi-1D jet state behind the shock propagating into the V-shaped profile with density equal to 0.25 in the center and 0.5 at the walls. The cross-section is taken at the distance from the shock approximately equal to 10 tube diameters.

crosses the path of the laser beam (see Fig. 4c). At this point, the density gradient is again aligned with the tube axis, and this "normal" portion of the shock causes another sudden jump in the laser deflection. Naturally, the distance between the first jump (caused by the central shock segment) and the second one (due to the near-wall parts of the shock) is greatest for the most bowed shock. In the case of shock reflection at the wall, a double modulation of this strong density jump can result. Such a double modulation was observed in both the experimental and computational data.

Ganguly et al. reported the laser deflection data as a function of time only until a decrease in density was indicated, namely the data was truncated as soon as the laser beam deflection crossed through 0. Fig. 7 shows the data in this more familiar (truncated and inverted) form, where the data is plotted on an inverted *x*-axis. The heated core temperature is lowest (highest density) for the bottom plot, and highest (lowest temperature) for the top plot. These runs have also been plotted at precisely the same times in order to allow comparison of the shock speeds. This can be done because shock acceleration is typically negligible beyond the transient onset of initial flow. Since each shock has an effectively constant velocity, the inverted plotting in space is equivalent to plotting the data as a function of the (scaled) time required for a fluid feature to pass a fixed diagnostic point. This is the quantity against which the experimental data was reported. With the same average density ahead of the shock for each of the different profiles, the shock speed and strength predicted by the 1D approximation is the same for all four distributions. This translates to the same expected time of arrival (or same distance traveled) for each of the four shocks. Fig. 7 shows that the shock through the deep/narrow profile travels the most quickly to arrive at the laser beam first, and the last shock wave to reach the laser beam (the slowest shock wave) is the one propagating through the shallowest/broadest profile. This demonstrates the need for more than a 1D model to understand this problem. The shock splitting increases as the central gas temperature is raised. For the highest central temperature,

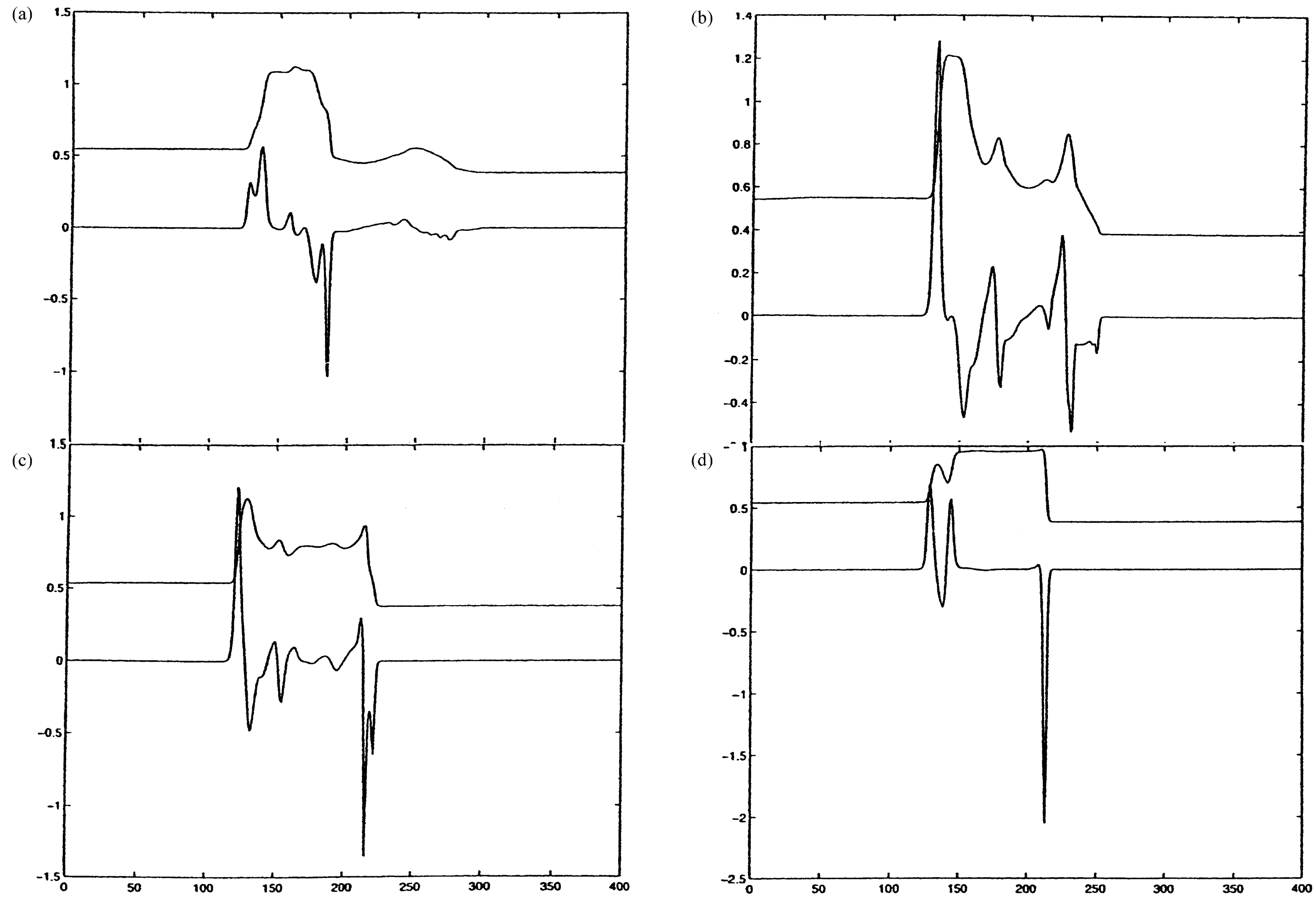

Fig. 6. The integrated over the cross-section density (top curve) and its derivative (bottom curve) as a function of longitudinal distance in four different simulations corresponding to four profiles shown in Fig. 4 and measured at the same instant of time.

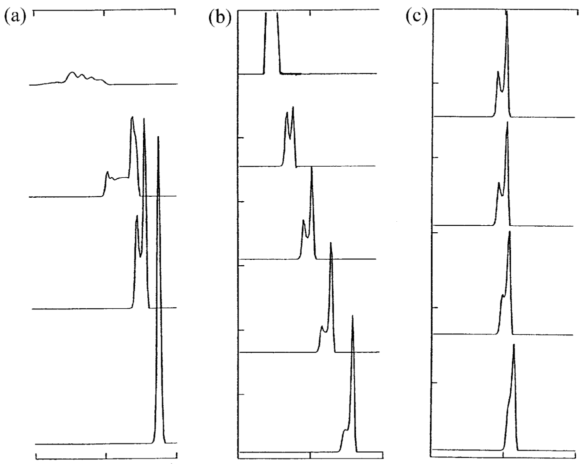

Fig. 7. Truncated and inverted versions (see the text) of the integrated density derivative shown in Fig. 6 mimicking the form in which experimental results were reported: (a) the top data set is from propagation into the narrowest of the profiles in Fig. 2A, the bottom is from propagation into the widest; (b) the top data set (which is a sharp peak extending beyond the top of the figure) is from propagation into the widest profile in Fig. 2B, the bottom is from propagation into the narrowest; (c) the top data set is from propagation into the top-hat profile of Fig. 2C, the bottom is from propagation into the V-shaped profile.

the shock seems to be nearly completely dissipated, which could (counter-intuitively) suggest a reduction of "total drag" in the confined shock tube geometry. This pitfall in interpretation emphasizes that, before drawing any conclusions from Fig. 7, Fig. 6 should be consulted, since it indicates the large mass of gas lagging far behind the significantly weakened leading shock, a feature which will also contribute to the dissipation budget. This information is lost if the data is truncated prematurely.

In the experiments, the gas temperature distribution is not well known. The top-hat profiles correspond to a situation in which a uniform electric current density flows through a central region of the gas, with a cooling gas flow along the tube to whisk the heat away. For a given total current, as the central current-carrying region becomes smaller, a correspondingly smaller amount of gas within that region carries a higher current density and therefore becomes hotter. The only evidence for such a narrow discontinuous temperature distribution in the experimental system is the filamentation which occurs at very high electric currents. In this case, the current is carried mainly through a very narrow region of strongest ionization similar to the narrowest of the top-hat profiles. Whereas no specific experiments were performed to capture precisely such conditions, it is interesting to see the effect of such strong heating on the shock wave. Deeper, thinner profiles correspond to increasingly hotter gas over a narrower region in the center of the tube. Given the coarse approximation that the gas at the walls is maintained at 300 K, the core temperatures can be estimated from the profiles of Fig. 2A. In this case, the central temperatures correspond to approximately 370, 600, 940 and 2470 K. The narrowest profile therefore resembles a hot, narrow filament/arc through the gas. Such an arc is what results in the experimental system as the electric current through the plasma is increased. However, no shocks were propagated (or observed) under such conditions.

Having looked at the above example to understand how the computational results relate to the experiments, it is important to consider the dependence of the shock dynamics on the exact density profile. One method of bridging the gap between the sharp gradient of the top-hat case and the shallow gradient of the V-shapes is to consider the sequence of profiles in Fig. 2C in which one gradually moves from the top-hat to the V-shape. In this case, the average density is once again kept at 0.375. The simulated "laser diagnostic" results are shown in Fig. 7c. Propagation through the V-shaped profile is shown on the bottom plot, and the initial (fore-shock) transverse density gradient increases with each successively higher plot, such that the top plot shows the results of propagation through the top-hat profile. This helps to identify the role of the steepness of the transverse density gradient on the behavior of the shock. The results show that a steeper gradient leads to a more pronounced splitting, with little effect on the shock speed.

To investigate the role of the profile width, given the strong splitting from the top-hat distribution, the profiles in Fig. 2B were studied. The splitting signatures are shown in Fig. 7b, where the successively higher plots show the results of propagation through the successively wider initial density profiles. As the central heated portion increased in width, the net average density ahead of the shock decreased. Alternatively, one can consider this to increase the net average temperature ahead of the shock. It follows that the average speed of sound ahead of the shock is also greater, which leads one to predict the increase in the shock speed shown in the results. The data also shows that the integrated density gradient at the leading edge of the shock can match that at the normal intersection of the shock with the tube wall when the respective "widths" of these regions are properly adjusted. This can be seen for the case in which the shock is "split" into two nearly equal jumps.

A Gaussian profile was also introduced, as a more moderate and physical profile than the two extreme transverse gradients of the V-shape and top-hat distributions. Comparisons of the shock splitting diagnostics (similar to Fig. 7) for the V-shape, Gaussian and the top-hat profiles are shown in Fig. 8. To see the effect of profile depth (heating), the central density was taken at values of 0.2, 0.15, 0.1 and 0.05, while maintaining the wall density at 0.5 for all of the above mentioned types of profiles. In these simulations, the fore-shock central density is smaller in the successively higher plots. It is interesting that the speed of the shock intersection with the wall (the large jump) stays relatively constant despite the increase in overall temperature. The main difference upon decreasing the central density is how far the leading edge of the shock leads the portion of the shock which intersects the wall. When comparing the results between the V-shape, Gaussian and top-hat profiles, the most significant differences become apparent when propagating into the very low initial central densities (very high central temperatures).

The less extreme profiles correspond to the regimes in which the experimental measurements have been made. In addition to the clear trend of sharper transverse density gradients resulting in sharper splitting, the gross features of the splitting signature also appear to be ubiquitous. This indicates a robustness of the features over the entire range of physically reasonable fore-shock density profiles. It further indicates that it may be possible to perform helpful and guiding simulations with only a few key pieces of information (e.g. the gas temperatures at the tube walls and on the tube axis). The results presented here can assist in identifying the key parameters which may be necessary to model effectively the shock dynamics.

4.2. *Vorticity*

The goal of this investigation was to determine the effect of the different fore-shock density profiles on ex-

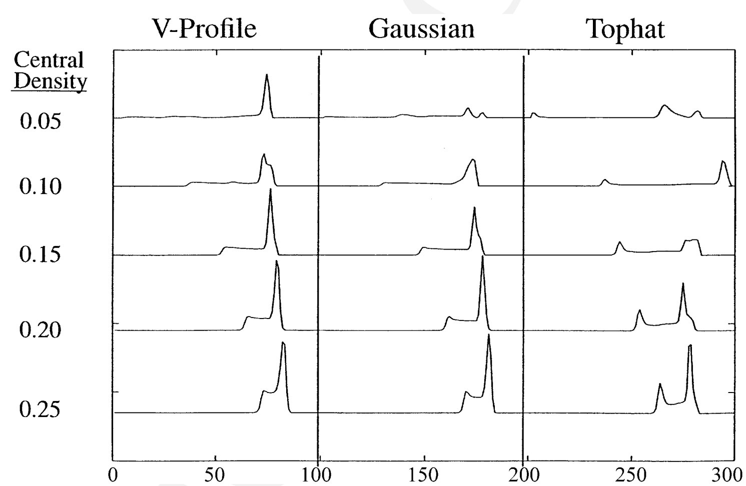

Fig. 8. Shock splitting diagnostic similar to Fig. 7 for three different types of initial density profiles (V-shaped, Gaussian and top-hat) with the value at the wall fixed at 0.5 and the value at the center taken to be 0.05, 0.1, 0.15, 0.20 and 0.25 (top to bottom curves).

perimentally measurable shock signatures and speeds. The vorticity was considered to be an important element in the dynamics and was therefore also studied.

As a shock wave propagates into an inhomogeneously heated gas, vorticity is generated baroclinically as calculated by (6). The strong pressure gradient of the shock wave and the density gradient ahead of the shock are effectively perpendicular to one another, which creates the jet-like flow described in Section 2.2. In 3D, the axial symmetry of the fore-shock density distribution in the shock tube ensures that the generated vorticity behind the shock is ring-like. In 2D, this is represented as dipolar vorticity. This generated dipolar vorticity is moved backward toward the trailing density discontinuity. It is interesting that, for sufficiently shallow fore-shock density gradients, an effectively constant (quasi-1D) fluid state is established immediately behind the shock, through which the generated vorticity "propagates backward". Such a 1D jet flow is shown in Fig. 5b and corresponding profiles of vorticity, density and pressure are shown in Fig. 5a, c and d correspondingly. Note that pressure is nearly constant across the jet which agrees with its stationarity and one-dimensionality. Upon reaching the lagging discontinuity (the analog of the contact surface in the 1D Riemann problem), the dipolar vorticity accumulates creating an unstable situation by interacting with a vortex sheet on the contact surface (described below). This heavy concentration of vorticity near and on the trailing density discontinuity can be seen in Fig. 9 which presents the vorticity fields at different times for the V-shaped initial profile. The subsequent evolution of vorticity is different for the top-hat and the V-shape as can be seen comparing Figs. 4d and

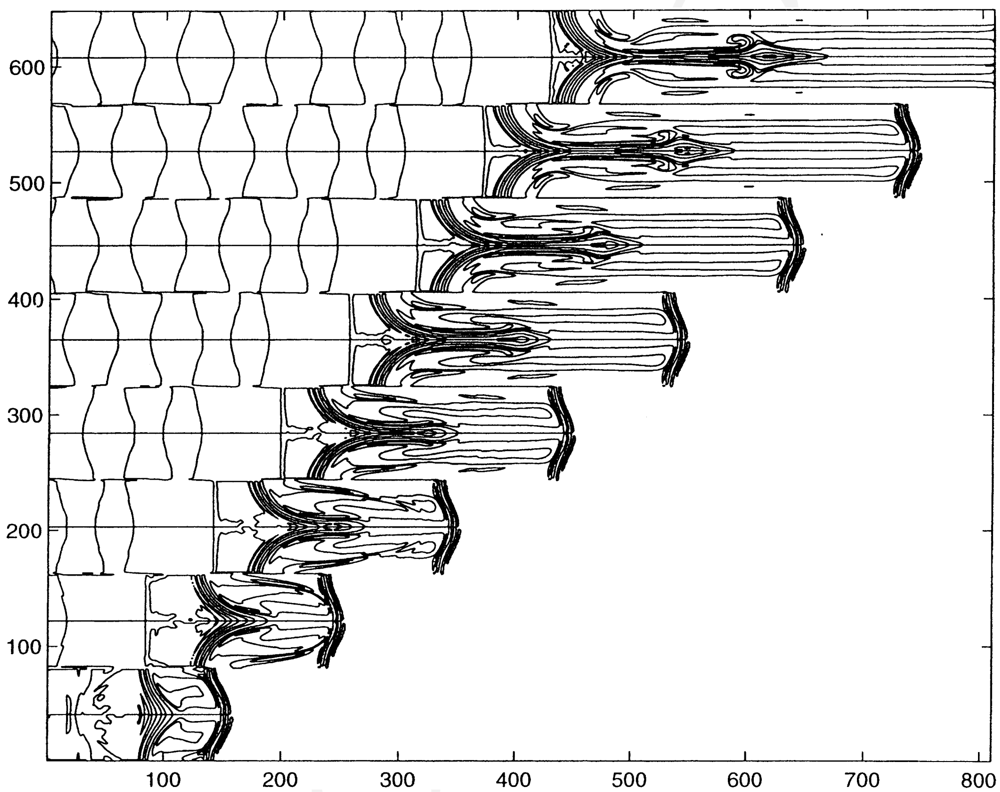

Fig. 9. Vorticity field for a shock propagating into the V-shaped profile (with density equal to 0.25 in the center and 0.5 at the walls) shown at eight different moments of time. Positive vorticity is generated on the shock's upper half and the negative vorticity is generated on its half. This vorticity propagates away from the shock forming a quasi-1D state (jet). The jet reflects off the trailing surface and advects an oppositely signed vorticity (generated near the trailing surface) back toward the shock.

9. In the top-hat case, vorticity tends to roll into a mushroom-like structure (discussed below), whereas in the V-shape case, vorticity squeezes itself into a thin elongated jet-like structure along the tube centerline and directed oppositely to the main jet.

Both the shock and the lagging discontinuity are acted on by forces due to the inhomogeneous density and jet-like flow. The shock maintains a type of "elasticity", due to the strong pressure drop across it. Indeed, the pressure forces acts to preserve its shape and to prevent its unbounded convective distortion. On the lagging discontinuity, the pressure jump is minimal which results in a much smaller elasticity. Indeed, in the corresponding 1D Riemann problem this would be a contact surface with zero pressure jump across it. Therefore, the lagging surface is, in effect, advected with the fluid nearly passively. Further, the strong dipolar vorticity near and on the lagging surface makes its evolution very similar to the nonlinear development of the Richtmyer–Meshkov instability [15,16] with its characteristic mushroom shape which is most pronounced in Fig. 4d.

The dynamics of the vorticity and density discontinuity are difficult to describe, since their interactions are strongly nonlinear. However, in both the V-shape and top-hat cases, the initial process at the "contact discontinuity" is straightforward. Just as occurs at the shock, the fact that $\vec{\nabla}P$ and $\vec{\nabla}\rho$ are not parallel, the trailing density discontinuity result in the generation of vorticity according to (6). Near the shock, there is a smooth, relatively weak $\vec{\nabla}\rho$ from the V-shaped density profile, whereas the shock provides a very strong (singular) $\vec{\nabla}P$. In contrast, at the trailing density discontinuity, the $\vec{\nabla}\rho$ term is strong and singular, while $\vec{\nabla}P$ is very weak (pointing upstream in the *x*-direction, as is the case at the shock). The amount of vorticity produced at the back density discontinuity is also smaller than the amount of vorticity produced at the shock. As the mushroom shape of the back density discontinuity evolves and its head curls over, regions develop where the sign of $\partial\rho/\partial y$ reverses, resulting in the generation of vorticity oriented oppositely of that generated at the shock. The velocity field corresponding to such an oppositely oriented vorticity is directed oppositely to the main jet and can be viewed as a jet recirculation. In other words, this oppositely oriented vorticity propagates in the opposite direction of that generated at the shock, when considered in the average restframe of the fluid behind the shock. It therefore propagates forward toward the shock wave, penetrating into the shock-generated vorticity which is propagating backward. These dynamics become much more apparent when the system is evolved for long times. Fig. 10 shows a vorticity field in the V-shape case which is an enlarged version of one of the frames presented in Fig. 9. It can be seen how the oppositely directed vorticity generated at the contact surface penetrates the 1D fluid state (including the vorticity field streaming back from the shock wave). The vorticity contours are shaded with the white being the most positive (out of the page), and the darkest colors being the most negative (into the page). By computing at different resolution levels we saw that the large-scale vorticity structure is a robust physical phenomenon, whereas the small-scale "wiggles" on it are more sensitive to the resolution level. However, these oscillations are likely to represent a true physical phenomenon, the Kelvin–Helmholtz instability which arises on the interface of two counter propagating jets.

4.3. Comparison to 1D theory

In this section, the V-shaped initial density profile was considered (see Fig. 2C). To compare the results of the 2D simulation with a simple 1D approximation, let us compare the following four cases:

a) A 1D shock propagating into a uniform density of 0.5 (the maximum density of the V-shaped distribution);
b) A 1D shock propagating into a uniform density of 0.375 (the average density of the V-shaped distribution). This represents the behavior predicted by the 1D theory;
c) A 1D shock propagating into a uniform density of 0.25 (the minimum density of the V-shaped distribution);
d) The cross-sectional average of the 2D simulation results for the shock propagating into the V-shaped density distribution.

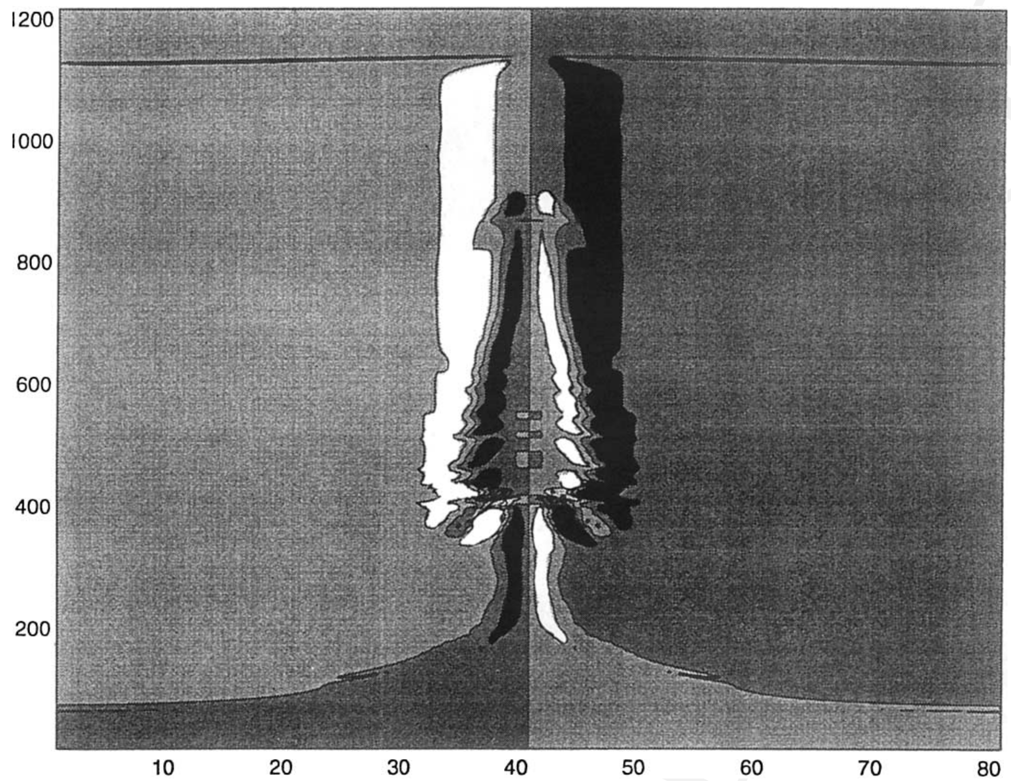

Fig. 10. Details of one of the vorticity frames from Fig. 9 showing the quasi-1D jet and the recirculating flow squeezing into its middle. Note fine oscillations on the recirculating jet which are due to the Kelvin–Helmholtz instability.

The results for shock propagation into the V-shaped density distribution (case c) differ significantly from the prediction of the 1D model (case b). In both the pressure and density distributions, the observed value just behind the shock is lower than that predicted by the 1D theory. The computed density is lower by approximately 15–20%, and the computed pressure is lower by approximately 10–15%. Toward the trailing density discontinuity, both the pressure and density do, however, rise continuously to values near those predicted by the 1D model. Another surprising feature is that the shock itself moves faster than expected, while the trailing density discontinuity moves slower than expected. In fact, the shock propagating into the V-shaped density profile moves at approximately the same speed as a shock propagating into a uniform gas of density 0.25 (case d); whereas the trailing density discontinuity in the V-shaped case moves at approximately the same speed as the contact surface of a shock propagating into a uniform density of 0.5 (case a). It is tempting to conclude that, although the speeds of interest can be roughly calculated using the average fore-shock density, the shock speed is modified by the deviation of the minimum fore-shock density from the average value. Similarly, the speed of the trailing density discontinuity is modified by the deviation of the maximum fore-shock density from the average value. Our results further suggest that the speed of the “contact surface” is dictated predominantly by the value of the maximum fore-shock density occurring at the shock-tube walls. Deriving a general rule for this will require a careful study and analysis. It is interesting to consider the possible role of momentum-carrying dipolar vorticity in this phenomenon by exploring a momentum-balance argument, which includes the momentum carried by the dipolar vorticity, to explain the increased shock speed and decreased contact surface speed. This would result in the shock wave gaining additional forward thrust by ejecting momentum-carrying dipolar (or “ring-like” in 3D) vorticity in the backward direction. The impact of this momentum-carrying vorticity on the trailing density discontinuity would impede the forward motion of this discontinuity, and hence reduce its speed. Momentum would therefore be transferred from the shock wave to the trailing contact surface, mediated by dipolar vorticity generated at the shock.

5. Conclusion

This paper discusses the propagation of a shock wave through a shock tube containing gas with one of several possible initial transverse density profiles. These transverse density profiles were made deeper and sharper to see the effect on shock bowing. It was found that the shock bowing can change dramatically with different initial transverse density profiles, and results were presented which strongly resemble the experimental observations of shock splitting reported for propagation through weakly ionized gases. Stronger transverse density gradients in the initial density profiles resulted in more pronounced shock splitting, and dramatic effects were observed at extremely high central gas temperatures. However, considering moderate heating, the basic shock splitting signatures, observed experimentally, were replicated very well by modeling the 2D fluid dynamics alone. Furthermore, these signatures are relatively insensitive to the exact shape of the initial transverse density distribution. A 1D state was observed behind the shock wave when propagating into sufficiently shallow density gradients, and an interesting interaction between the contact surface and the vorticity generated by the shock was also noted. We emphasize again the key role played by vorticity when shocks interact with temperature gradients.

As it was mentioned in the introduction to this paper and in the previous literature, the study of the shock tube experiments helps understanding the drag reduction mechanisms in the wind tunnel experiments of the Klimov’s group [1,2]. However, the differences in geometry are far too great to be able to directly apply our results in this case and computations of more realistic 2D and 3D flows remain to be done. Further, many of these experiments were performed in dilute bi-molecular gases and to model these flows realistically one has to include effects of the rotational and vibrational degrees of freedom and, at higher Mach numbers, the radiative thermoconductivity and ionization.

Acknowledgements

We thank Vladimir Zakharov for many fruitful discussions. This work was supported by the United States Air Force Office of Scientific Research. The authors also acknowledge the Engineering and Physical Sciences Research Council, British Aerospace, and the Defense Evaluation and Research Agency of the UK for their additional support and collaboration.

References

[1] A.I. Klimov, A.N. Koblov, G.I. Mishin, Yu.L. Serov, I.P. Yavor, Sov. Tech. Phys. Lett. 8 (4) (1982) 192–194.
[2] A.I. Klimov, A.N. Koblov, G.I. Mishin, Yu.L. Serov, K.V. Khodataev, I.P. Yavor, Sov. Tech. Phys. Lett. 8 (5) (1982) 240–241.
[3] US AFOSR Workshop on Weakly Ionized Gases Proceedings, June 9–13, 1997.
[4] B. Ganguly, P. Bletzinger, A. Garscadden, Phys. Lett. A 230 (1997) 218–222.
[5] K. Kremeyer, S. Nazarenko, A. Newell, AIAA 2000-2700, 31st AIAA Plasmadynamics and Lasers, and Fluids 2000 Conferences, Denver, June 19–22, 2000.
[6] K. Kremeyer, S. Nazarenko, A. Newell, AIAA 99-0871, 37th AIAA Aerospace Sciences Meeting and Exhibit, Reno, 1999.
[7] Y.K. Ionikh, N.V. Chernysheva, A.P. Yalin, S.O. Macharet, L. Martinelli, R.B. Miles, AIAA 2000-0714, 38th AIAA Aerospace Sciences Meeting and Exhibit, Reno, 2000.
[8] G. Sod, J. Comput. Phys. 27 (1978) 1–31.
[9] R. Courant, K.O. Friedrichs, Supersonic Flow and Shock Waves, Springer, Berlin, 1976.
[10] W. Hilbun, W. Bailey, AFIT, Private communication, 1997.
[11] P.G. Saffman, Vortex Dynamics, Cambridge University Press, Cambridge, 1992.
[12] G.-S. Jiang, C.-W. Shu, J. Comput. Phys. 126 (1996) 202–228.
[13] G.-S. Jiang, C.-C. Wu, J. Comput. Phys. 150 (1999) 561–594.
[14] T. Cain, Defence evaluation and research agency, ministry of defense, UK, Private communication, 1998.
[15] J.W. Jacobs, J. Fluid Mech. 234 (1992) 629–649.
[16] N.J. Zabusky, Ann. Rev. Fluid Mech. 31 (1999) 495–535.